THE JOURNAL OF BIOLOGICAL CHEMISTRY VOL. 289, NO. 15, pp. 10668–10679, April 11, 2014
Published in the U.S.A.

Long-chain Acyl-CoA Dehydrogenase Deficiency as a Cause of Pulmonary Surfactant Dysfunction*

Received for publication, December 3, 2013, and in revised form, February 21, 2014 Published, JBC Papers in Press, March 3, 2014, DOI 10.1074/jbc.M113.540260

Eric S. Goetzman[‡§1], John F. Alcorn[‡], Sivakama S. Bharathi[‡], Radha Uppala[‡], Kevin J. McHugh[‡], Beata Kosmider[¶], Rimei Chen[‖], Yi Y. Zuo[‖2], Megan E. Beck[§], Richard W. McKinney[‡], Helen Skilling[‡], Kristen R. Suhrie[‡], Anuradha Karunanidhi[‡], Renita Yeasted[‡], Chikara Otsubo[‡], Bryon Ellis[**], Yulia Y. Tyurina[‡‡§§], Valerian E. Kagan[‡‡§§], Rama K. Mallampalli[¶¶3], and Jerry Vockley[‡§]**

From the [‡]Department of Pediatrics, University of Pittsburgh School of Medicine, Children's Hospital of Pittsburgh of University of Pittsburgh School of Medicine, Pittsburgh, Pennsylvania 15224, the [§]Department of Human Genetics, Graduate School of Public Health, University of Pittsburgh, Pittsburgh, Pennsylvania 15213, the [¶]Department of Medicine, National Jewish Health, Denver, Colorado 80206, the [‖]Department of Mechanical Engineering, University of Hawaii at Manoa, Honolulu, Hawaii 96822, the [**]Department of Medicine, Acute Lung Injury Center of Excellence, University of Pittsburgh, Pittsburgh, Pennsylvania 15213, the [‡‡]Center for Free Radical and Antioxidant Health and [§§]Department of Environmental and Occupational Health, University of Pittsburgh, Pittsburgh, Pennsylvania 15260, and the [¶¶]Medical Specialty Service Line, Veterans Affairs Pittsburgh Healthcare System, Pittsburgh, Pennsylvania 15213

Background: The contribution of long-chain acyl-CoA dehydrogenase (LCAD) to human fatty acid oxidation is not understood.
Results: LCAD localizes to lung alveolar type II cells, which produce pulmonary surfactant; LCAD-deficient mice have surfactant dysfunction.
Conclusion: LCAD is important for lung energy metabolism and lung function.
Significance: LCAD may play a role in human lung disease and unexplained sudden infant death.

Long-chain acyl-CoA dehydrogenase (LCAD) is a mitochondrial fatty acid oxidation enzyme whose expression in humans is low or absent in organs known to utilize fatty acids for energy such as heart, muscle, and liver. This study demonstrates localization of LCAD to human alveolar type II pneumocytes, which synthesize and secrete pulmonary surfactant. The physiological role of LCAD and the fatty acid oxidation pathway in lung was subsequently studied using LCAD knock-out mice. Lung fatty acid oxidation was reduced in LCAD$^{-/-}$ mice. LCAD$^{-/-}$ mice demonstrated reduced pulmonary compliance, but histological examination of lung tissue revealed no obvious signs of inflammation or pathology. The changes in lung mechanics were found to be due to pulmonary surfactant dysfunction. Large aggregate surfactant isolated from LCAD$^{-/-}$ mouse lavage fluid had significantly reduced phospholipid content as well as alterations in the acyl chain composition of phosphatidylcholine and phosphatidylglycerol. LCAD$^{-/-}$ surfactant demonstrated functional abnormalities when subjected to dynamic compression-expansion cycling on a constrained drop surfactometer. Serum albumin, which has been shown to degrade and inactivate pulmonary surfactant, was significantly increased in LCAD$^{-/-}$ lavage fluid, suggesting increased epithelial permeability. Finally, we identified two cases of sudden unexplained infant death where no lung LCAD antigen was detectable. Both infants were homozygous for an amino acid changing polymorphism (K333Q). These findings for the first time identify the fatty acid oxidation pathway and LCAD in particular as factors contributing to the pathophysiology of pulmonary disease.

Mitochondrial fatty acid oxidation (FAO)[4] is an important energy-producing pathway that requires the concerted effort of more than 20 enzymes (1, 2). First, carnitine palmitoyltransferase-1, carnitine-acylcarnitine translocase, and carnitine palmitoyltransferase-2 facilitate the carnitine-dependent transport of long-chain fatty acids across the outer and inner mitochondrial membranes. Once inside the mitochondria, fatty acids are re-conjugated to CoA and degraded to two-carbon units (acetyl-CoA) by repeated cycling through four enzymatic steps of β-oxidation. The first of these enzymatic steps is catalyzed by a family of five acyl-CoA dehydrogenases (ACADs) as follows: short-chain acyl-CoA dehydrogenase; medium chain acyl-CoA dehydrogenase (MCAD); long-chain acyl-CoA dehydrogenase (LCAD); very long-chain acyl-CoA dehydrogenase (VLCAD), and acyl-CoA dehydrogenase-9 (ACAD9). Genetic deficiencies of short-chain ACAD, MCAD, VLCAD, and ACAD9 are well described and are among the most common inborn errors of metabolism (3, 4). In contrast, no disease-

* This work was supported, in whole or in part, by National Institutes of Health Grants DK090242 (to E. S. G.) and DK78775 (to J. V.) from NIDDK and Grants HL107380 (to J. F. A.), HL096376, HL097376, and HL098174 (to R. K. M.), P01 HL114453 (to R. K. M. and V. E. K.) from NHLBI.
[1] To whom correspondence should be addressed: 4401 Penn Ave., Rangos 5117, Pittsburgh, PA 15224. Tel.: 412-692-7952; Fax: 412-692-7816; E-mail: eric.goetzman@chp.edu.
[2] Supported by National Science Foundation Grant CBET-1254795.
[3] Supported by a merit review award from the Department of Veterans Affairs.

[4] The abbreviations used are: FAO, fatty acid β-oxidation; LCAD, long-chain acyl-CoA dehydrogenase; ACAD, acyl-CoA dehydrogenase; MCAD, medium-chain acyl-CoA dehydrogenase; VLCAD, very long-chain acyl-CoA dehydrogenase; ACAD9, acyl-CoA dehydrogenase-9; ATII, alveolar type II pneumocytes; PLA$_2$, phospholipase A$_2$; ETF, electron-transferring flavoprotein; ATI, alveolar type I pneumocytes; PC, phosphatidylcholine; PG, phosphatidylglycerol; RDS, respiratory distress syndrome.

causing mutations have been identified for LCAD, and its role in human metabolism remains obscure.

In vitro, the substrate specificity of LCAD overlaps with that of VLCAD and ACAD9. All three enzymes have strong activity toward long-chain acyl-CoAs (14–20 carbons in length) (4). Additionally, LCAD has been shown to dehydrogenate branched-chain acyl-CoA substrates (5). VLCAD expression predominates in tissues that are known to rely upon fatty acids for energy such as liver, heart, and muscle. Correspondingly, VLCAD deficiency causes life-threatening metabolic decompensation, cardiomyopathy, and muscle weakness (6, 7). ACAD9 is also expressed in muscle and heart and is the only ACAD enzyme expressed at high levels in the brain and central nervous system (4). Additionally, ACAD9 interacts with complex I of the respiratory chain and may have other functions besides its ACAD activity (8, 9). In contrast to VLCAD and ACAD9, LCAD expression is low or nearly absent in liver, heart, and muscle and most abundant in lung, kidney, thyroid, and prostate (4, 10, 11).

The presence of the LCAD protein has been confirmed in human lung using immunostaining (4). In cultured primary human alveolar type II pneumocytes (ATII), influenza infection was found to down-regulate LCAD mRNA, whereas other FAO genes were not affected (12). Similarly, based on microarray studies in lung tumors, LCAD was included in a core set of genes whose expression levels distinguish cancerous from normal tissue (13). These reports prompted us to hypothesize that LCAD may play a role in fatty acid metabolism specific to lung. In this study, we confirmed localization of LCAD to human ATII cells. ATII cells are highly specialized cells in the alveolar epithelium that synthesize and secrete pulmonary surfactant. Surfactant is a mixture of phospholipids, cholesterol, and protein that allows for decreased surface tension at the air-liquid interface of the lung, preventing alveolar collapse and allowing for normal gas exchange. We further observed surfactant deficiency and altered lung mechanics in LCAD-deficient mice. Based on these findings, it is postulated that LCAD deficiency in humans may manifest primarily as a lung disease rather than resembling other FAO disorders.

EXPERIMENTAL PROCEDURES

Human Tissues, Cell Isolation, and Cell Culture—Post-mortem human lung tissues from children who suffered unexplained deaths during the 1st year of life were acquired through the University of Maryland Tissue Bank. Primary human ATII cells and bronchial epithelial cells were isolated from adult donor lungs not suitable for transplantation as described (14). Briefly, the right middle lobe was perfused, lavaged, and instilled with elastase (Roche Diagnostics). The tissue was minced, and ATII cells were purified by centrifugation through an Optiprep gradient (Accurate Chemical Scientific, Westbury, NY) followed by negative selection with CD14-coated magnetic beads (Dynal Biotech, Oslo, Norway) and binding to IgG-coated dishes (Sigma). The resulting ATII cell cultures were then either maintained as differentiated ATII cells for 6 days as described (15) or trans-differentiated into ATI-like cells by culturing for 2 days in DMEM with 10% FBS on rat tail collagen-coated plates followed by 4 days in DMEM with 5% FBS (16).

The A549 human alveolar adenocarcinoma cell line and the MLE12 transformed murine lung epithelial cell line were from ATCC, and they were cultured as described previously (17).

Animals—All breeding and experimental protocols were approved by the University of Pittsburgh Institutional Animal Care and Use Committee. LCAD$^{+/-}$ mice (B6.129S6-*Acadl*^{tm1Uab}) were purchased from the Mutant Mouse Regional Resource Center (University of Missouri, Columbia, MO). LCAD$^{-/-}$ mice were backcrossed to C57Bl/6 but became infertile. Thus, the LCAD$^{-/-}$ mice used here were maintained on a mixed C57Bl/6 and 129S6 background. Wild-type and homozygous mutant littermates were identified from initial heterozygous crosses and used to establish separate breeding colonies of wild-type and homozygous mutant mice. All studies used age- and sex-matched animals.

Immunoblotting of Tissue, Cell Lysates, and Lavage Fluid—Frozen lung tissue was homogenized in 50 mM Tris-HCl, pH 8.0, 2 mM EDTA, and 0.25% lubrol detergent, pH 8.0, with protease inhibitors and incubated on ice for 15 min. Cultured cells were lysed in RIPA buffer. Both tissue and cell homogenates were cleared by centrifugation and analyzed for protein concentration in triplicate using the Bradford method (Bio-Rad). Lysates were electrophoresed and transferred to nitrocellulose membranes using the Bio-Rad Criterion apparatus. Anti-LCAD, VLCAD, and ACAD9 antibodies, generated previously in our laboratory, were used as described (18). Anti-actin antibody (Santa Cruz Biotechnology, Dallas, TX) was used as a loading control. In comparisons of different cell types (Fig. 1*b*), both actin and GAPDH were unsuitable as loading controls due to differential expression between cell types. In this case, equal loading between lanes was verified using Ponceau S staining of the nitrocellulose membranes following transfer. For Western blots of lavage fluid, the abundance of albumin and phospholipase A_2 (PLA_2) per volume of fluid was determined by blotting either 10 μl of fluid from each animal for albumin or, in the case of PLA_2, by dialyzing/concentrating 800 μl of lavage fluid from each animal to 10–20 μl prior to loading onto the gel. Anti-mouse albumin (Sigma) and anti-PLA_2 (Santa Cruz Biotechnology) were both used at 1:1000.

ACAD Enzyme Activity—Frozen tissue was homogenized in 50 mM Tris-HCl, 2 mM EDTA, pH 8.0. Lubrol detergent was added to 0.25% w/v. After 15 min of incubation on ice, the samples were centrifuged, and supernatants used for ACAD enzyme activity measurements using the anaerobic electron transfer flavoprotein (ETF) fluorescence reduction assay were as described previously (19). Briefly, tissue homogenate and pure ETF were incubated together in a sealed, degassed quartz cuvette at 32 °C in a heated cuvette block, and the enzymatic reaction was started by the addition of either palmitoyl-CoA or oleoyl-CoA (Sigma) at a final concentration of 25 μM. The decrease in ETF fluorescence was followed for 60 s using a Jasco fluorescence spectrophotometer. Activity was calculated with 1 milliunit of activity defined as the amount of enzyme necessary to completely reduce 1 nmol of ETF in 1 min. Final activity values were calculated as milliunits of activity/mg of total protein used in the reaction.

Analysis of Free Coenzyme-A—Freshly harvested samples of mouse brown adipose tissue, liver, and lung were weighed and

snap-frozen in liquid nitrogen. The frozen tissue pieces were homogenized in perchloric acid using a Bullet Blender (Next Advance, Averill Park, NY). Following centrifugation, the supernatants were neutralized to pH 6.0 and applied to a Luna C18(2) column (Phenomenex, Torrance, CA) using a Waters HPLC. Free CoA was separated following the chromatographic conditions described by DeBuysere and Olson (20). Three concentrations of pure CoA (Sigma) were injected as standards, and the peak heights were used to generate a standard curve. The concentration of CoA in tissue samples was expressed as nanomoles/mg of tissue.

Radiolabeled Fatty Acid Oxidation—Rates of FAO were determined by tritium release using [9,10-^{3}H]palmitic and [^{3}H]oleic acids (PerkinElmer Life Sciences) or [2,3-^{3}H]octanoic acid (American Radiolabeled Chemicals, St. Louis, MO). Sodium salts of ^{3}H-fatty acids were mixed with their corresponding unlabeled fatty acids in ethanol. The ethanol was driven off by a gentle stream of nitrogen, and the fatty acids were reconstituted in PBS/BSA to a concentration of 500 μM (4× stock at 10 μCi per ml). Following three 10-s cycles of sonication in a sonicating water bath, the mixtures were placed on a rotator at 37 °C for 4 h to allow conjugation of the fatty acid to BSA. ^{3}H-Fatty acid/BSA stocks were frozen at −20 °C and used within 1 month. Tissues were collected early in the light cycle into ice-cold PBS, 5 mM glucose and minced into ~10-mg pieces. Approximately 50 mg of each tissue was placed into wells of a 24-well tissue culture plate containing 300 μl of PBS, 5 mM glucose supplemented with 1 mM carnitine and 125 μM final concentration of labeled fatty acid-BSA. In some experiments, lung explants were preincubated in media supplemented with 100 μM of the irreversible carnitine palmitoyltransferase-1 inhibitor etomoxir (or DMSO vehicle for control) for 30 min prior to the experiment. The plates were incubated at 37 °C for 1 h. The tissue pieces and reaction buffer were then transferred into Eppendorf tubes on ice and homogenized using a Bullet Blender (Next Advance, Averill Park, NY). A 10-μl portion of homogenate was set aside for protein determination (D_c reagent, Bio-Rad). For [^{3}H]palmitic and [^{3}H]oleic acids, ^3H_2O and water-soluble β-oxidation products (*i.e.* acetyl-CoA) were separated from the lung homogenate and excess labeled fatty acid substrate by chloroform/methanol extraction following the method of Bligh and Dyer (21). The aqueous layer was removed and subjected to liquid scintillation counting. For [^{3}H]octanoic acid, ^3H_2O was separated using Dowex resin as described (18).

Pulmonary Function Testing—Respiratory mechanics were measured as described previously (22). Briefly, mice were anesthetized with pentobarbital sodium (90 mg/kg i.p.). After tracheotomy with a modified 18-gauge intravenous adapter, the mice were attached to a computer-controlled piston ventilator (FlexiVent, SCIREQ, Montreal, Quebec, Canada) and ventilated with a tidal volume of 0.2 ml and 3 cm of H_2O positive end-expiratory pressure. Multiple linear regression was used to fit measured pressure and volume in each individual mouse to the model of linear motion of the lung (23). Model fits that resulted in a coefficient of determination <0.80 were excluded. Pressure volume analysis was completed in a series of stepwise volume inflation and deflation with a maximum lung pressure of 30 cm of H_2O. Dose-response curves to inhaled methacholine were determined as described (22) using 0.75, 3.125, 12.5, and 50 mg/ml methacholine. Airway resistance, tissue resistance, and tissue elastance were measured. The peak response for each variable was determined, and the percent change from baseline was calculated.

Lung Histology—Three 6-week-old mice of each genotype were sacrificed by pentobarbital overdose followed by exsanguination through the renal artery. The lungs were inflated with 10% neutral-buffered formalin (Sigma) at a pressure of 25 cm of H_2O for 10 min, removed from the animal, and placed in fresh 10% neutral-buffered formalin for 24 h before processing and paraffin embedding. H&E-stained 5-μm sections were scored by a pathologist blind to the genotype of the tissues.

Bronchoalveolar Lavage Fluid Collection and Analysis—All lavage fluids analyzed for these studies were collected from nonventilated 5–6-week-old mice. Mice were anesthetized and tracheotomized as described above. Bronchoalveolar lavage was performed using three 1-ml aliquots of 0.9% NaCl. The amount of saline recovered was carefully measured and then centrifuged at 300 × *g* for 10 min to pellet cells, which were immediately resuspended in PBS, centrifuged onto glass slides, and stained for differential counting. The cell-free lavage supernatants were removed and either frozen at −80 °C or, for some experiments, subjected to centrifugation at 40,000 × *g* for 15 min to pellet large aggregate surfactant, which was used for constrained drop surfactometry and phospholipid analyses. Within 1 month, lavage supernatants were thawed and analyzed for protein concentration (Bio-Rad), and phosphatidylcholine (PC) content using thin layer chromatography followed by the phosphorus assay as described (24, 25). For some experiments, large aggregate surfactant pellets were resuspended in 200 μl of saline and extracted with chloroform/methanol, and the organic layer was collected and used for the phosphorus assay.

Constrained Drop Surfactometry—The constrained drop surfactometer is a newly developed droplet-based surface tensiometer (26–28). Large aggregate surfactant pellets, obtained as described above, were gently dispersed into 0.9% NaCl, 1.5 mM $CaCl_2$, and 2.5 mM HEPES, pH 7.0, with a final phospholipid concentration of ~1.0 mg/ml. An ~10-μl droplet was dispensed onto the drop holder. After drop formation, the surface tension was recorded and found to quickly decrease to an equilibrium value of ~22–25 millinewton/m. Once the equilibrium was established, the droplet was compressed and expanded at a rate of 3 s per cycle with a compression ratio controlled to be less than 50% of the initial surface area. At least five compression-expansion cycles were studied for each droplet. As with surfactant cycling in captive bubble surfactometers, the cycles became repeatable after the first cycle and were quantified with the minimum surface tension (γ_{min}), maximum surface tension (γ_{max}), and compression ratio required to reach γ_{min} (CR_{min}) (29, 30). The entire measurements were conducted under physiological conditions in an environmentally controlled chamber. Drop images were taken at a rate of 10 frames/s. The surface tension, surface area, and drop volume were determined with axisymmetric drop shape analysis (31).

LC/MS Analysis of Phospholipid Molecular Species—Lipids were extracted using the Folch procedure (32), and the phospholipid classes were separated by high performance thin layer chromatography as described (33). The PC and phosphatidylglycerol (PG) classes were recovered, and lipid phosphorus was determined by a micro-method (34). LC/MS was performed using the Dionex Ultimate^{TM} 3000 HPLC system coupled online to a linear ion trap mass spectrometer (LXQ ThermoFisher) as described (33).

Incorporation of Radiolabeled Fatty Acid and Choline into Phospholipids—Lung explants were collected and incubated with [^{14}C]palmitate/BSA (125 μM) as described above but for 2 h. The tissue pieces were washed vigorously four times in cold PBS to remove excess labeled fatty acid/BSA, homogenized, and extracted by the method of Bligh and Dyer (21). The aqueous layer was discarded, and the organic layer was dried under a gently stream of nitrogen. The organic layer was reconstituted in 1 ml of chloroform, and phospholipids were separated from neutral lipids using disposable 50-mg silica SPE columns exactly as described (35). The eluates were reduced in volume to ~100 μl by a gentle stream of nitrogen and then subjected to liquid scintillation counting. For [^{3}H]choline incorporation, explants were incubated for 3 h at 37 °C in serum-free DMEM in the presence of [^{3}H]choline. The tissue explants were homogenized and extracted as above, and incorporation of [^{3}H]choline into the lipid fraction was determined by scintillation counting. For experiments with MLE12 cells, the cells were grown to ~80% confluency in 24-well plates. FAO was measured in PBS supplemented with 1 mM carnitine and 125 μM [^{3}H]palmitate/BSA ± 100 nM etomoxir. After 2 h, the media were collected and extracted by the method of Bligh and Dyer, and the aqueous layer containing ^3H_2O was counted. For choline incorporation, MLE12 growth media was supplemented with 1 μCi per well of [^{3}H]choline. After 6 h, the cells were lysed with 0.6 N NaOH. Radiolabeled lipids were isolated (21) and subjected to liquid scintillation counting. Incorporation of [^{3}H]choline was normalized to cellular protein content for both lung tissue explants and MLE12 lysates.

Phospholipase A_2 Activity— PLA_2 activity was measured in cell-free lavage fluid using a plate-based assay kit from Cayman Chemical (Ann Arbor, MI) following the manufacturer's instructions.

LCAD Gene Sequencing and Quantitative PCR—Genomic DNA and total RNA were isolated from frozen lung tissue using commercial kits (Qiagen, Germantown, MD). Genomic DNA was used as template for PCR using primer sets flanking each exon. PCR products were gel-isolated, purified, and subjected to sequencing. To quantify LCAD mRNA, total RNA was used for reverse transcription followed by quantitative PCR with an Applied Biosystems 7300 Real Time PCR System and SYBR Green (Applied Biosystems, Carlsbad, CA).

Statistical Analyses—Results are given as the mean ± S.D. Statistical analyses represent two-tailed Student's *t* tests, and null hypotheses were rejected at 0.05.

Ethical Approvals—The use of animals and human tissues was approved by the Institutional Animal Care and Use Committee and Institutional Review Board, respectively, at the University of Pittsburgh.

RESULTS

LCAD Expression in Human Lung Localizes to the Alveolar Epithelium—To extend a previous observation of LCAD mRNA in human lung (4), we investigated the presence of the LCAD protein in human lung biopsies and various lung-derived primary cells. Western blotting readily detected LCAD in human post-mortem lung tissue at levels comparable with wild-type mouse lung (Fig. 1*a*). Next, Western blotting was used to investigate LCAD expression in several major lung cell types. LCAD antigen was not detected in primary human lung microvascular endothelial cells or in primary human lung fibroblasts (data not shown) but was robustly expressed in primary human ATII cells (Fig. 1*b*). LCAD is clearly enriched in ATII cells as evidenced by Western blotting equal amounts of ATII cell lysate *versus* total lung tissue homogenate from the same individuals. Interestingly, LCAD is not expressed in A549 human lung adenocarcinoma cells, which are often used as a model of ATII cells, but is expressed in the murine lung epithelial cell line MLE12 (Fig. 1*b*). In contrast to isolated ATII cells, clear detection of LCAD in lung tissue homogenates requires 10 times higher protein loading (50 μg in Fig. 1*a versus* 5 μg in *b*). Moreover, primary human bronchial epithelial cells showed weak LCAD expression visualized only upon extended exposure to film indicating that not all lung epithelial cell types express LCAD equally (Fig. 1*b*, *middle panel*). ATI cells, which are morphologically and functionally distinct from ATII cells but are thought to arise from ATII cells (16), are difficult to isolate from human lungs. However, ATI-like cells can be differentiated from ATII cells in culture, as evidenced by changes in morphology and the attainment of ATI marker proteins such as caveolin-1 (Fig. 1*c*) (16). In this trans-differentiation model, we observed that LCAD expression is reduced by about half in ATII cells after 6 days of culture (Fig. 1*d*). LCAD expression is approximately equal between ATII cells cultured for 6 days and the same cells trans-differentiated into ATI-like cells (Fig. 1*d*). Together, these data indicate that LCAD localizes specifically to alveolar epithelial cells.

Lung Tissue Oxidizes Fatty Acids at a High Rate—We next established that the mitochondrial FAO pathway is active in mouse lung using liver as a control tissue. Total ACAD activity toward palmitoyl-CoA was ~40% lower in lung than liver (Fig. 2*a*). This represents the combined activities of LCAD, VLCAD, and ACAD9. Surprisingly, the level of free CoA, which is thought to be rate-limiting for mitochondrial FAO (1, 36), was very low in lung compared with liver and brown adipose tissue (Fig. 2*b*). Yet, despite low levels of CoA, β-oxidation of palmitate and oleate was readily detected in lung explants, and the rate of FAO matched or exceeded the rate in liver explants (Fig. 2, *c* and *d*). The rate of nonmitochondrial FAO was also significantly higher in lung as determined by measuring residual palmitate oxidation in the presence of etomoxir, an irreversible inhibitor of carnitine palmitoyltransferase-1 (Fig. 2*c*). Etomoxir-insensitive FAO is usually attributed to peroxisomes (37).

LCAD$^{-/-}$ Mouse Lungs Demonstrate Significantly Reduced Long-chain FAO—Western blotting confirmed the absence of LCAD antigen in lung homogenates prepared from LCAD$^{-/-}$

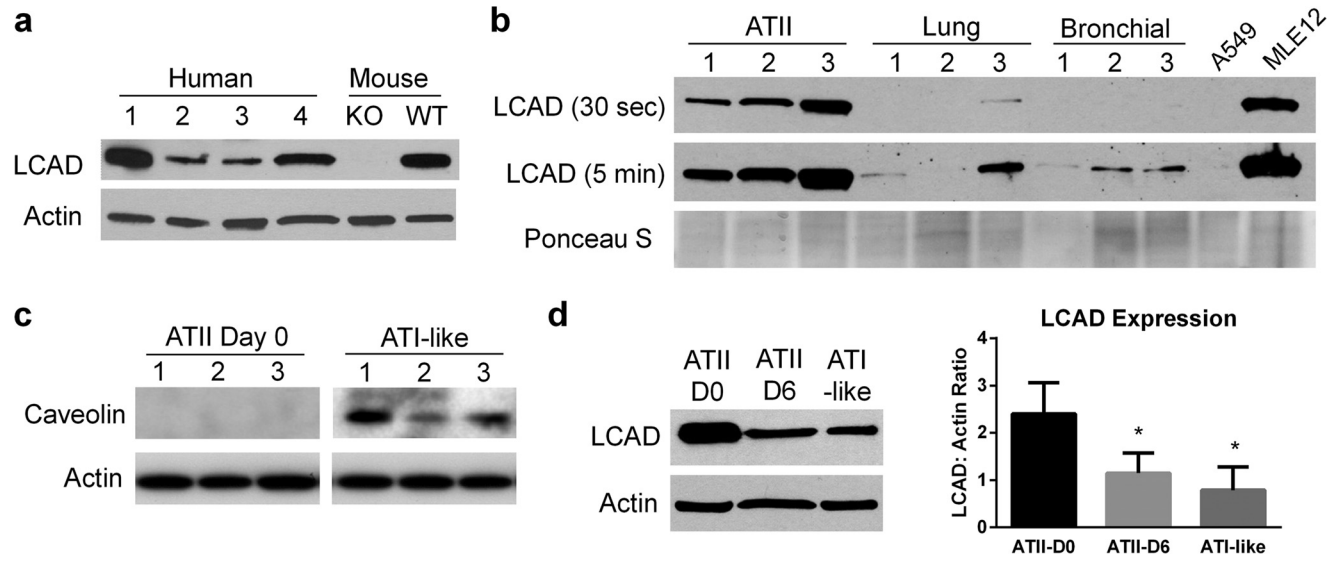

FIGURE 1. **LCAD expression in human lung localizes to ATII cells.** *a,* Western blotting of LCAD in 50 μg of total protein from four human post-mortem lung tissue extracts *versus* 50 μg of total protein from LCAD$^{-/-}$ and wild-type mouse lung extracts indicates similar levels of total LCAD antigen between human and mouse lungs. *b,* Western blotting for LCAD in 5 μg of extracts prepared from isolated primary human type II alveolar epithelial cells (*ATII*, *lanes 1–3*) *versus* 5 μg of lung tissue homogenate from the same individuals (*Lung*, *lanes 1–3*), and 5 μg of primary bronchial epithelial cell lysates (*Bronchial*, *lanes 1–3*, not from the same individuals as in the other *lanes*). *Lanes A549* and *MLE12* contain 25 μg of lysates from the A549 (human) and MLE12 (mouse) cell lines, which are often used as models of ATII cells. LCAD expression is only visualized in 5 μg of lung homogenates or bronchial cell lysates after a long exposure to film (*middle panel*). Actin and GAPDH were differentially expressed between the different cell types, and thus Ponceau S staining of the blot is shown as a loading control (*bottom panel*). *c,* caveolin-1 expression, a marker of AT1 cells, in 5 μg of lysate from freshly isolated ATII cells *versus* the same cells trans-differentiated into ATI-like cells. *d,* representative Western blot comparing LCAD antigen levels in 5 μg of extract prepared from freshly isolated ATII cells (*D0*) *versus* the same cells after 6 days in culture (*D6*) or after trans-differentiation into ATI-like cells. The *bar graph* represents the means ± S.D. of LCAD normalized to actin in three sets of D0, D6, and ATI-like cells. *, $p < 0.05$ *versus* ATII-D0.

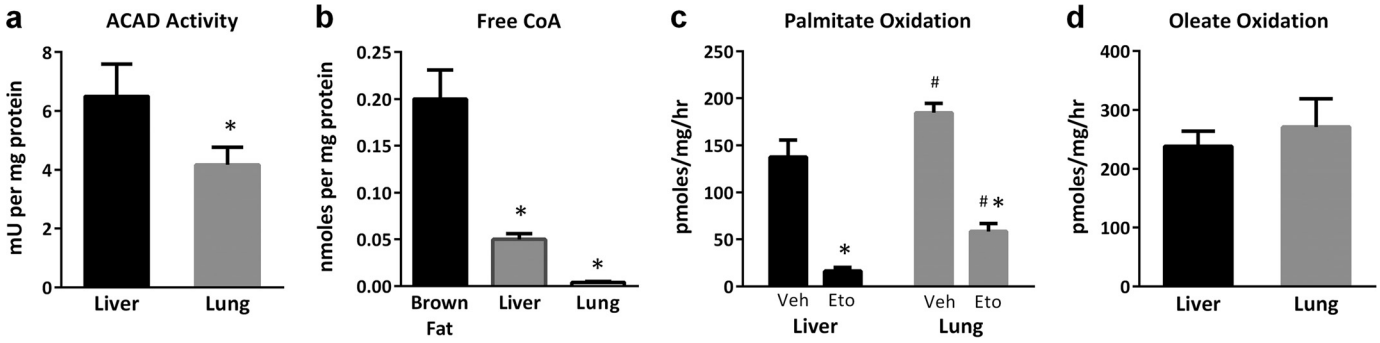

FIGURE 2. **Lung tissue oxidizes fatty acids at a high rate.** All *graphs* depict means ± S.D. *a,* acyl-CoA dehydrogenase enzyme activity toward palmitoyl-CoA (combined activities of LCAD, VLCAD, and ACAD9) was determined in lung and liver tissue homogenates. $n = 5$ mice per group; *, $p < 0.01$. *b,* free co-enzyme A, an essential cofactor for mitochondrial FAO, was measured in mouse tissue extracts using HPLC. Liver and lung both have much lower CoA levels than brown adipose tissue. $n = 3$ mice, *, $p < 0.01$. *c,* [^{3}H]palmitate (C16:0) oxidation in minced lung *versus* liver ($n = 4$ mice). Tissues were treated with etomoxir (*Eto*) as an inhibitor of mitochondrial FAO or DMSO vehicle (*Veh*). Etomoxir-insensitive FAO is considered peroxisomal in origin. *, $p < 0.01$ for etomoxir *versus* vehicle; #, $p < 0.01$ for lung *versus* liver. *d,* [^{3}H]oleate, an unsaturated fatty acid (C18:1), is oxidized at comparable rates between mouse liver and lung explants ($n = 4$ mice).

mice (Fig. 3*a*). VLCAD and ACAD9, which also dehydrogenate long-chain acyl-CoAs, were slightly increased in the LCAD$^{-/-}$ lung as observed by Western blot, but these changes did not reach statistical significance (Fig. 3*b*). Total long-chain ACAD activity in lung homogenates from LCAD$^{-/-}$ mice was reduced by 50 and 40% with palmitoyl-CoA and oleoyl-CoA as substrates, respectively (Fig. 3*c*). Accordingly, flux through the FAO pathway as measured with radiolabeled palmitate and oleate was also significantly reduced in lung explants from LCAD$^{-/-}$ mice (Fig. 3*d*). However, oxidation of octanoate (C8), a medium-chain fatty acid that is not a substrate for LCAD, was not reduced in LCAD$^{-/-}$ lung explants (Fig. 3*e*).

LCAD$^{-/-}$ Mice Have Altered Lung Mechanics—Lung function in nonstressed LCAD$^{-/-}$ mice was determined using a mechanical ventilator (FlexiVent). First, baseline values for the parameters of central airway resistance, tissue resistance, and tissue elastance were measured. Modest but statistically significant changes were seen in baseline lung tissue resistance and elastance in LCAD$^{-/-}$ mice, although central airway resistance was not altered (Fig. 4*a*). Thus, LCAD$^{-/-}$ lungs are stiffer and more difficult to inflate, with greater elastic recoil. To determine whether these changes were associated with airway hyper-responsiveness, another cohort of animals was subjected to methacholine-induced bronchoconstriction. LCAD$^{-/-}$ and wild-type mice responded similarly to increasing doses of methacholine with regard to central airway resistance and tissue elastance (data not shown). LCAD$^{-/-}$ mice were hyporesponsive on the tissue resistance parameter (Fig. 4*b*), indicating that the change in baseline lung mechanics is not likely due to heightened airway responsiveness. Similarly, H&E-stained

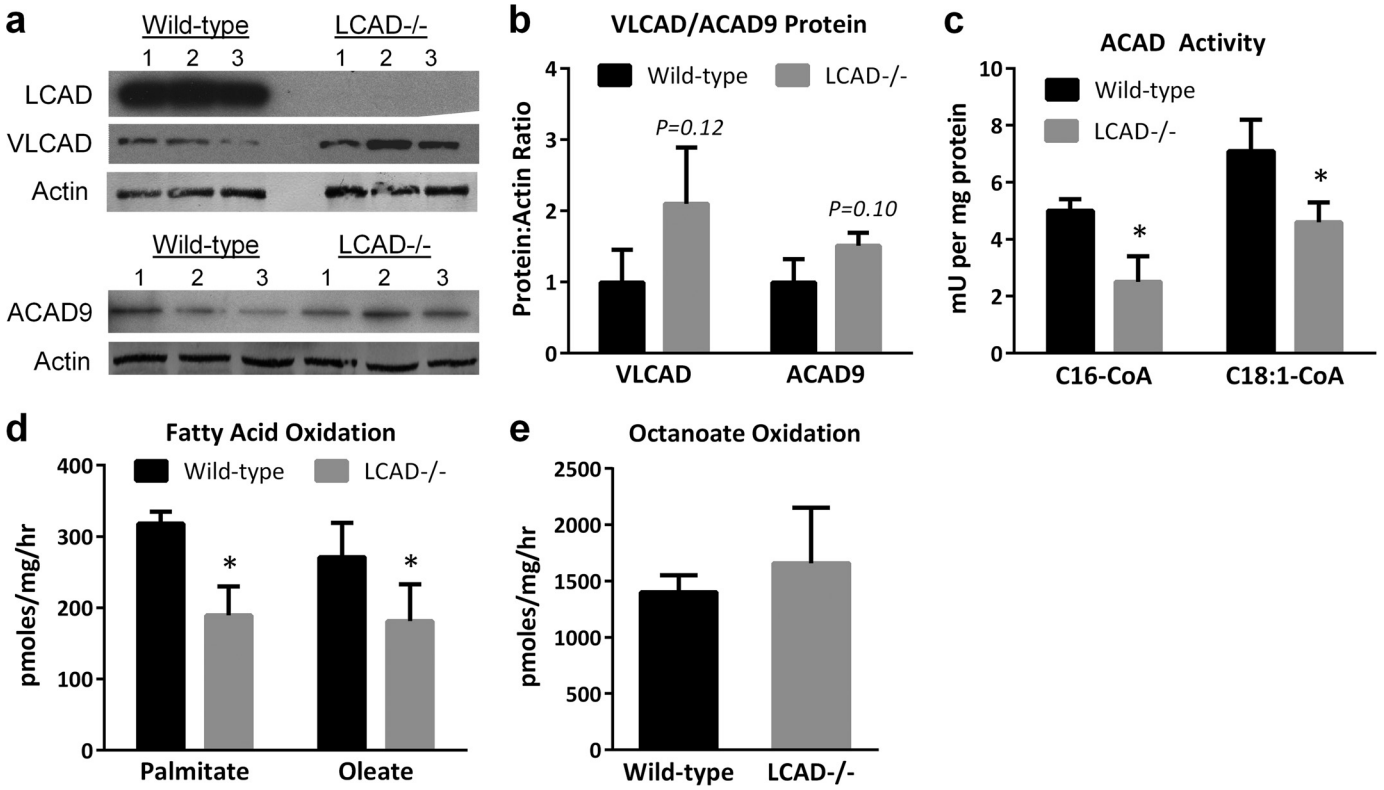

FIGURE 3. **LCAD$^{-/-}$ mouse lungs demonstrate significantly reduced FAO.** All *graphs* depict means ± S.D. *a,* Western blotting for all three long-chain ACAD enzymes in mouse lung extracts (50 μg; $n = 3$ mice). *b,* densitometric analysis of the blots shown in *a*, with expression normalized to actin. *c,* total ACAD activity toward palmitoyl-CoA (C16:0) and oleoyl-CoA (C18:1) is significantly reduced in lung homogenates from LCAD$^{-/-}$ mice ($n = 4$ mice; *, $p < 0.01$). Correspondingly, *d,* rates of [^{3}H]palmitate and [^{3}H]oleate oxidation by LCAD$^{-/-}$ lung explants are significantly reduced ($n = 4$ mice; *, $p < 0.01$). *e,* oxidation of [^{3}H]octanoate (C8), a substrate for MCAD but not LCAD, is not altered in LCAD$^{-/-}$ mice ($n = 3$ mice).

sections of lung tissue from LCAD$^{-/-}$ mice did not show obvious signs of pathology or the presence of immune cells (Fig. 4*c*), eliminating chronic inflammation as the cause of the altered lung mechanics.

Pressure-volume curves were analyzed to calculate static compliance and hysteresis. Pulmonary compliance was significantly reduced in LCAD$^{-/-}$ mice, again indicating stiff lungs that are more difficult to inflate (Fig. 4*d*). Consistent with altered breathing mechanics, the area under the pressure-volume curves during inspiration *versus* expiration (hysteresis) was significantly greater in LCAD$^{-/-}$ mice (Fig. 4*e*).

Lavage Fluid from LCAD$^{-/-}$ Mice Shows Increased Protein Content and Decreased Phosphatidylcholine—The epithelial lining fluid at the tissue-air interface in alveoli contains pulmonary surfactant, immune cells, and many proteins either secreted by the lung epithelium or transported across the epithelial barrier from blood (38, 39). Epithelial lining fluid was collected from LCAD$^{-/-}$ mice by bronchoalveolar lavage with saline. The amount of saline recovered during lavage was recorded and was not significantly different between genotypes. Immune cells were collected from lavage fluid by centrifugation, stained, and counted. As typical for immunologically naive mice, only alveolar macrophages were observed, with significantly fewer recovered from LCAD$^{-/-}$ mice (Fig. 5*a*). The cell-free supernatant from LCAD$^{-/-}$ mice contained significantly more total protein (Fig. 5*b*) and more serum albumin per ml (Fig. 5*c*) suggesting increased epithelial permeability to serum proteins. Next, the concentration of total PC, the major surfactant phospholipid component, was measured and found to be reduced in lavage fluid from LCAD$^{-/-}$ mice (Fig. 5*d*).

Amount and Function of Pulmonary Surfactant Is Reduced in LCAD$^{-/-}$ Mice—To further investigate the possibility of surfactant deficiency in LCAD$^{-/-}$ mice, lavage fluids were subjected to centrifugation to isolate the large aggregate, surface-active surfactant fraction (40). The amount of phospholipids in the large aggregate fraction was determined using a phosphorus assay and was found to be significantly reduced in LCAD$^{-/-}$ mice (Fig. 6*a*). Next, lipid extracts from large aggregate surfactant were subjected to high performance thin layer chromatography followed by mass spectrometry to quantify the molecular species of PC and PG, which are the major phospholipid classes in surfactant. Several species showed significant differences between genotypes, and these are listed in Table 1. LCAD$^{-/-}$ mice displayed reduced dipalmitoyl (C16:0/C16:0)-PC concomitant with increased abundance of PC species with longer and unsaturated acyl chains. Similar changes were seen for PG. To determine whether these changes in composition alter surfactant function, the biophysical properties of the large aggregate surfactant were investigated using a constrained drop surfactometer (28). Surfactant from wild-type and LCAD$^{-/-}$ mice was subjected to compression-expansion cycles at a rate of 3 s per cycle, which mimics the rate of human breathing (mice breathe ~10× faster). Surface tension was monitored during the dynamic cycling. The maximum and minimum surface tensions achieved during cycling did not differ between genotypes of mice (Fig. 6, *b* and *c*). However, LCAD$^{-/-}$ surfactant showed

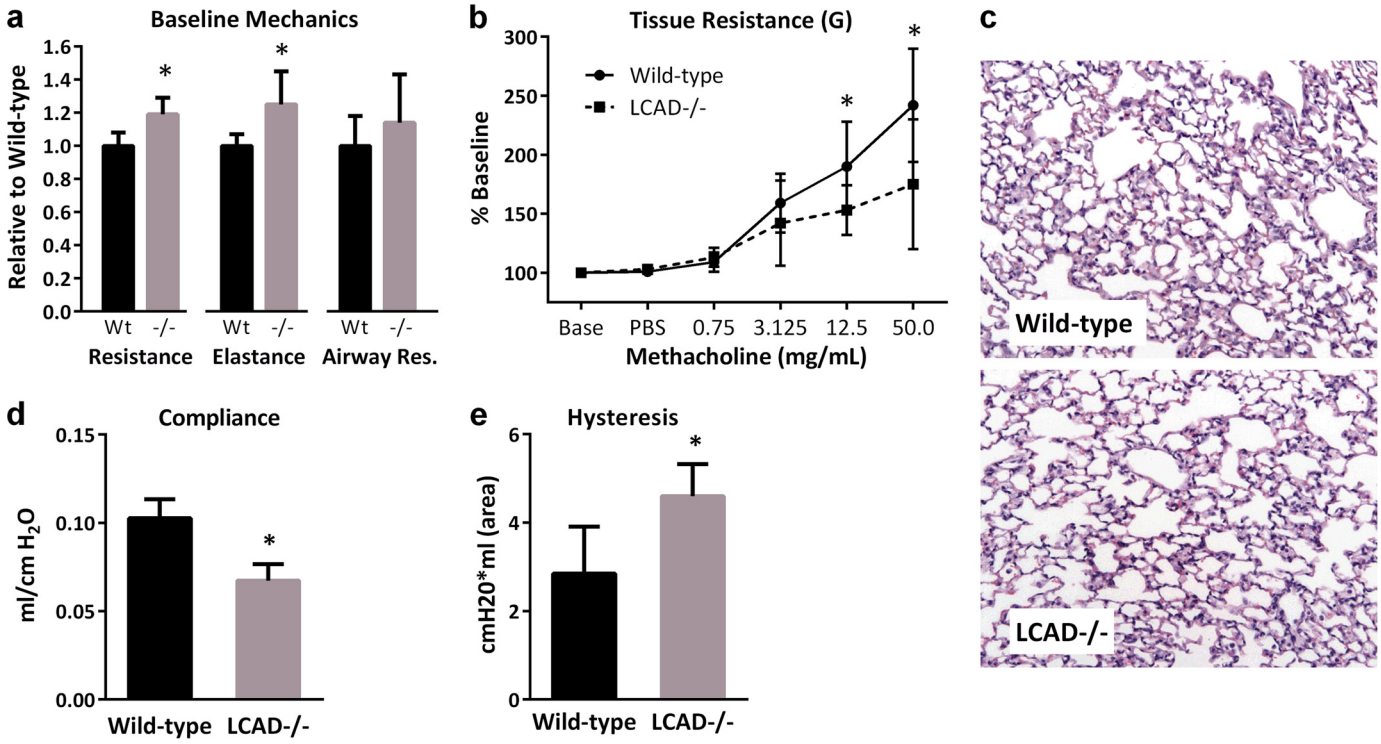

FIGURE 4. **LCAD$^{-/-}$ mice have altered lung mechanics.** All *graphs* depict means ± S.D. *a,* baseline lung mechanics in unstressed wild-type (+/+) *versus* LCAD knock-out (−/−) mice as determined by FlexiVent. A total of 15 animals was measured over two sessions, and the data were combined by normalizing to the mean of the +/+ mice in each session. *, $p < 0.05$. *b,* LCAD$^{-/-}$ mice are hypo-responsive to methacholine on the FlexiVent tissue resistance (*G*) parameter. Mice ($n = 5$) were challenged with increasing doses of methacholine during mechanical ventilation by FlexiVent. The elastance and airway resistance variables were the same between genotypes (data not shown); *, $p < 0.05$. *c,* representative H&E-stained lung sections from an LCAD$^{-/-}$ mouse and a wild-type control mouse. LCAD$^{-/-}$ lung shows no obvious signs of pathology. *d* and *e,* pulmonary compliance ($n = 8$) and hysteresis ($n = 8$) were significantly lower and higher, respectively in LCAD$^{-/-}$ mice; *, $p < 0.05$.

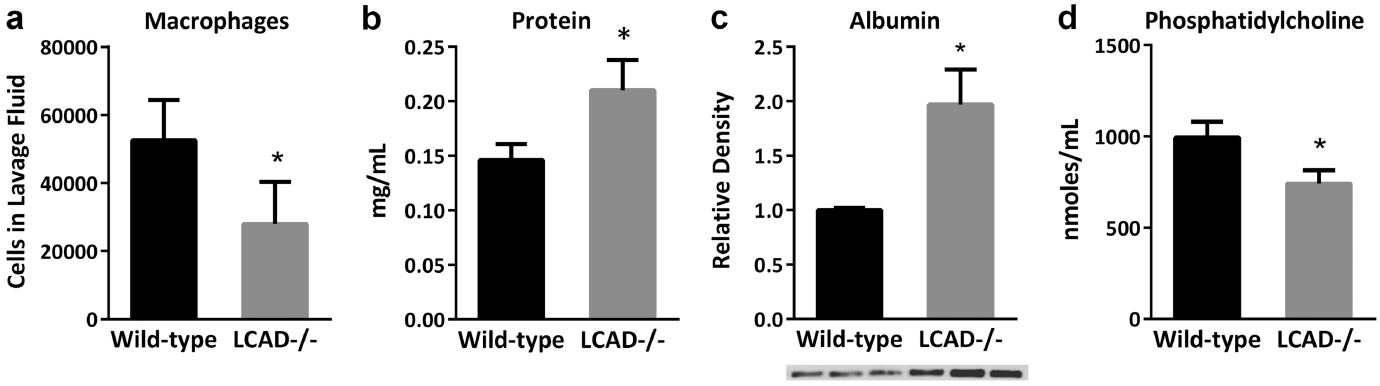

FIGURE 5. **Lavage fluid from LCAD$^{-/-}$ mice shows increased protein content and decreased phosphatidylcholine.** All *bar graphs* represent means ± S.D. *a,* mice ($n = 4$) were lavaged with three 1-ml aliquots of saline, and immune cells were collected by centrifugation, counted, and stained. Macrophages were the only cell type observed in both genotypes. *, $p < 0.05$. *b,* cell-free supernatant was subjected to assay for protein concentration. *, $p < 0.01$. *c,* equal volumes of cell-free supernatant were electrophoresed and blotted with anti-albumin antibody. Densitometry was used to quantify the levels of albumin that are shown in the *bar graph*; a representative blot is shown *below* the *bar graph*. *, $p < 0.01$. *d,* lipids were extracted from lavage fluids and subjected to TLC, and the phosphatidylcholine spots were scraped from the plate and analyzed by phosphorus assay ($n = 4$ mice). *, $p < 0.05$. All of these measures (*a*–*d*) were repeated in a second cohort of mice with similar results.

higher compressibility, requiring greater compression to reach minimum surface tension (Fig. 6*d*). Similarly, the surface tension measured at a 20% compression ratio of the surface area, considered to mimic alveolar compression during breathing (41), was significantly higher in LCAD$^{-/-}$ mice (Fig. 6*e*).

LCAD$^{-/-}$ Lung Explants Synthesize Phospholipids Normally—Synthesis and trafficking of surfactant is an energy-consuming process (42), and we hypothesized that reduced mitochondrial energy metabolism in LCAD$^{-/-}$ lung might limit surfactant synthesis. To test this hypothesis, the incorporation of radiolabeled palmitate and choline into phospholipids was measured in fresh lung explants from wild-type and LCAD$^{-/-}$ mice. Using either substrate, equal rates of phospholipid synthesis were observed between genotypes of mice (Fig. 7, *a* and *b*). Because lung tissue explants include many other cell types besides ATII, we sought to mimic LCAD deficiency *in vitro* in the murine ATII cell line MLE12 using the FAO inhibitor etomoxir. Etomoxir inhibited [^{3}H]palmitate oxidation by 75% in

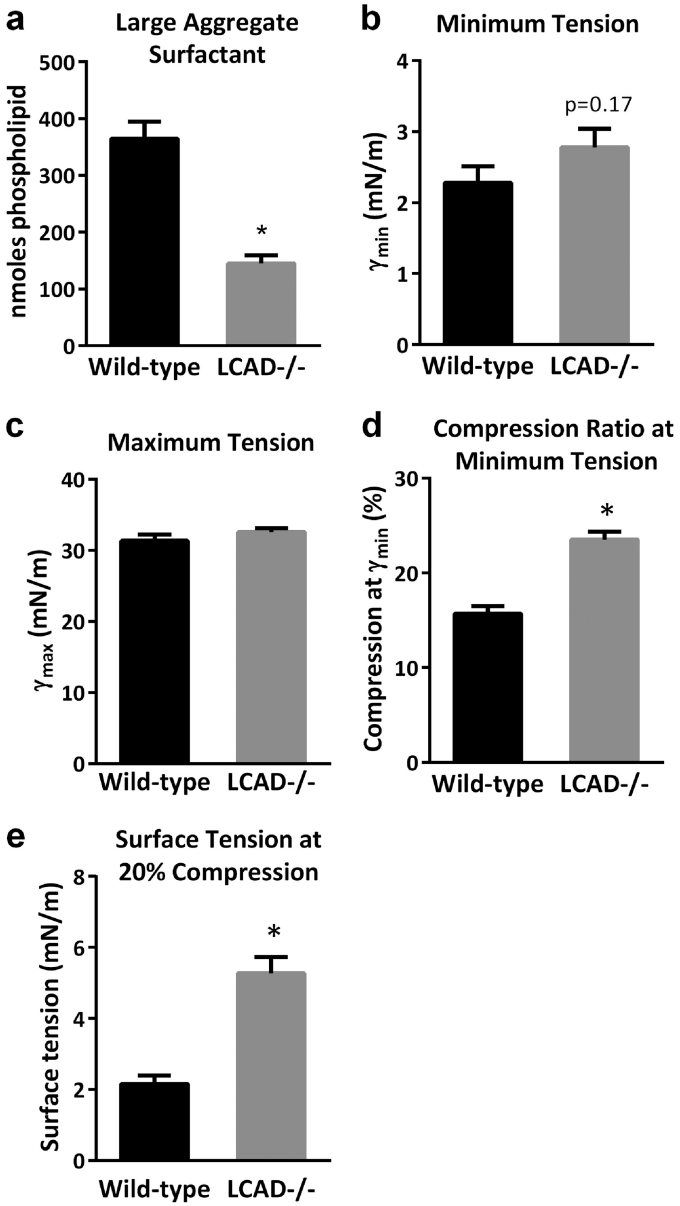

FIGURE 6. **Amount and function of pulmonary surfactant is reduced in LCAD$^{-/-}$ mice.** *a,* large aggregate, surface-active pulmonary surfactant was isolated from lavage fluid ($n = 4$ mice). Total lipids were extracted from the large aggregate material, and phospholipids were quantified by phosphorus assay. Shown are means ± S.D. *, $p < 0.01$. *b–e*, large aggregate material was assayed for surfactant function on a constrained drop surfactometer. Phospholipid concentrations were adjusted to 1.0 mg/ml, and the samples were dynamically cycled at varying compression ratios. Three mice of each genotype were analyzed in triplicate, and the *bar graphs* represent means ± S.E. *b* and *c,* minimum and maximum surface tensions achieved during cycling did not differ between genotypes. *d,* LCAD$^{-/-}$ mouse surfactant showed greater compressibility as demonstrated by requiring a higher compression ratio to reach minimum surface tension. *, $p < 0.01$. *e,* surface tension at a physiological compression ratio (20%) is significantly higher in LCAD$^{-/-}$ surfactant. *, $p < 0.01$.

TABLE 1
Molecular species of PC and PG in large aggregate surfactant fraction

Molecular species	Phosphatidylcholine		Phosphatidylglycerol	
	Wild type	LCAD$^{-/-}$	Wild type	LCAD$^{-/-}$
	pmol/nmol	*pmol/nmol*		
C14:0/C16:1[a]	4.8 ± 0.5	9.3 ± 0.5[b]	1.0 ± 0.3	2.0 ± 0.2[b]
C14:0/C16:0	82.6 ± 4.9	70.4 ± 19.1	14.7 ± 2.2	12.8 ± 1.0
C16:1/C16:1[a]	8.3 ± 1.0	8.6 ± 0.8	ND	
C16:0/C16:1	171.3 ± 6.9	180.2 ± 11.0	69.2 ± 3.9	64.0 ± 3.3
C16:0/C16:0	317.5 ± 12.0	274.7 ± 9.7[b]	140.6 ± 17.1	93.1 ± 14.8[b]
C16:1/C18:2[a]	4.4 ± 0.3	5.3 ± 0.5[b]	9.8 ± 0.8	10.6 ± 0.6
C16:0/C18:2	69.1 ± 1.4	85.2 ± 0.6[b]	220.8 ± 3.7	255.7 ± 8.8[b]
C16:0/C18:1	116.8 ± 5.1	116.7 ± 4.0	248.2 ± 5.0	249.8 ± 4.8
C16:1/C20:4[a]	9.3 ± 0.6	10.3 ± 0.7	8.2 ± 1.1	6.9 ± 0.9
C16:0/C20.4	50.2 ± 4.7	52.9 ± 3.2	59.6 ± 4.5	51.4 ± 3.5
C18:2/C18:2				
C18:1/C18:2[a]	5.7 ± 0.6	9.1 ± 0.5[b]	12.0 ± 1.5	23.8 ± 2.0[b]
C16:0/C20:2	11.7 ± 2.2	17.5 ± 1.1[b]	28.0 ± 3.7	47.0 ± 2.9[b]
C18:1/C18:1				
C18:0/C18:2				
C18:0/C18:1	ND		17.3 ± 1.5	23.8 ± 1.4[b]
C16:0/C22:6	71.2 ± 4.3	67.6 ± 2.9	93.8 ± 8.2	88.0 ± 5.2
C18:2/C20:4				
C16:0/C22:5	24.8 ± 2.0	30.6 ± 10.3	32.3 ± 3.5	28.9 ± 1.8
C18:1/C20:4				
C18:0/C20:4	24.0 ± 2.9	28.8 ± 2.5[c]	24.5 ± 1.8	21.5 ± 1.2
C18:1/C22:6[a]	2.7 ± 0.4	3.9 ± 0.3[b]	3.3 ± 0.5	4.2 ± 0.7
C18:0/C22:6	24.1 ± 2.1	27.1 ± 2.1[c]	13.8 ± 1.9	13.6 ± 1.6

[a] This is the suggested molecular species.
[b] p value is <0.01 *versus* wild type; ND indicates species not detected.
[c] p value is <0.05 *versus* wild type.

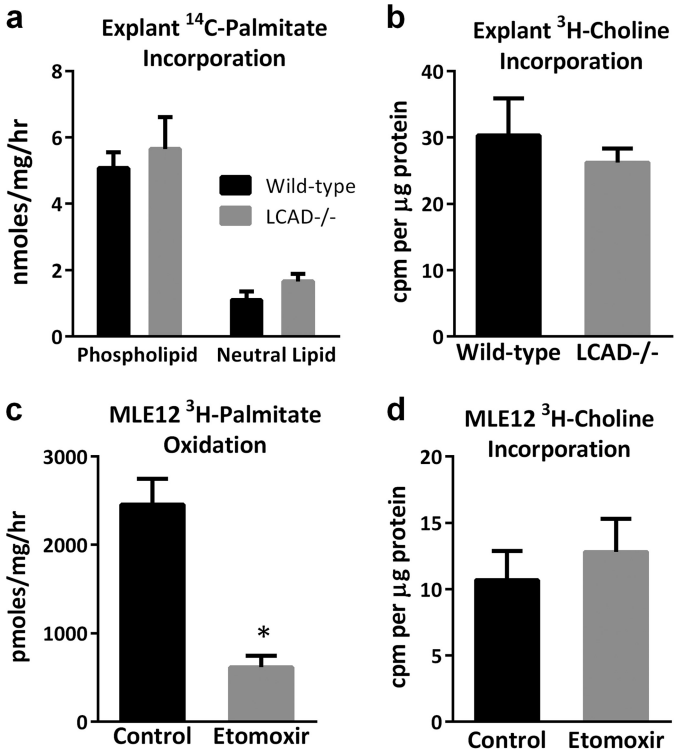

FIGURE 7. **LCAD$^{-/-}$ lung explants synthesize phospholipids normally.** *a,* fresh lung explants were incubated in serum-free DMEM supplemented with [^{14}C]palmitate. Total lipids were extracted and separated into neutral *versus* phospholipid fractions ($n = 4$). *b,* lung explants were incubated in serum-free DMEM in the presence of [^{3}H]choline, and incorporation of [^{3}H]choline into total lipids was determined. *c,* to model an FAO deficiency *in vitro*, etomoxir was used to inhibit palmitate oxidation in cultured MLE12 murine alveolar epithelial cells. *, $p < 0.01$. *d,* effect of etomoxir on [^{3}H]choline into total lipids was determined. All *bar graphs* depict means ± S.D.

MLE12 cells (Fig. 7*c*). However, etomoxir inhibition of FAO had no effect on [^{3}H]choline incorporation into the intracellular lipid fraction (Fig. 7*d*).

Increased surfactant degradation could also cause the observed reduction in surfactant phospholipids. Secreted PLA_2 is a known mechanism of surfactant degradation that has been implicated in respiratory diseases (43, 44). PLA_2 activity in lavage fluid from LCAD$^{-/-}$ and wild-type mice was very low in both genotypes and could not be accurately determined. Likewise, PLA_2 was difficult to detect by Western blotting of lavage

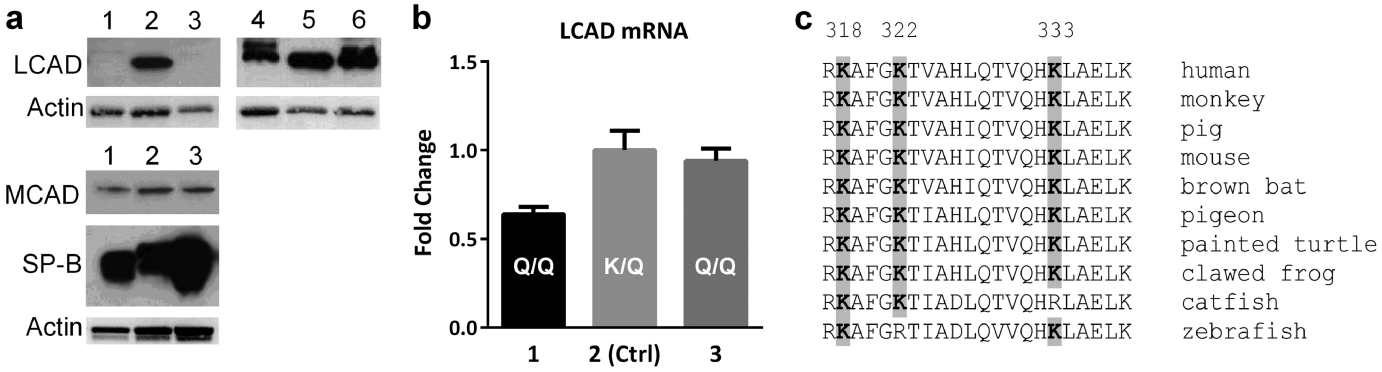

FIGURE 8. **Loss of LCAD antigen in two cases of sudden unexplained infant death.** *a,* anti-LCAD Western blotting of 50 μg of total protein extract prepared from post-mortem lung tissues from six children who suffered sudden deaths in the 1st year of life. The extracts from Cases 1 to 3 were further evaluated for MCAD and surfactant protein-B (*SP-B*) precursor expression. *b,* quantitative PCR was used to compare LCAD mRNA levels between Cases 1–3, normalized to Case 2 as a normal control. Sequencing of genomic DNA revealed the presence of the K333Q polymorphism; the genotype of each case with regard to this polymorphism is indicated on the *bars* with *white font*. *c,* Lys-333 is just downstream of two lysines (Lys-318/Lys-322) known to be regulated by reversible acetylation (69) and is highly conserved across species.

fluid and was only sporadically observed in fluids from both genotypes (blots not shown). These data pointing to low PLA_2 in both genotypes of mice, although not conclusive, suggest that PLA_2 is not the mechanism behind reduced lung function in $LCAD^{-/-}$ mice.

Loss of LCAD Antigen in Two Cases of Sudden Unexplained Infant Death—We postulate that LCAD may play a role in human lung pathophysiology. Disorders of fatty acid metabolism have previously been linked to sudden infant death syndrome (45). We used Western blotting to evaluate LCAD antigen in samples of lung from six infants who suffered unexplained deaths under the age of 1 year. Two of the six infants had no detectable LCAD antigen (Fig. 8*a*). The two samples of infant lung with no detectable LCAD were both positive for MCAD, a closely related enzyme to LCAD, as well as surfactant protein-B expression demonstrating the presence of ATII cells in the archived lung materials (Fig. 8*a*, *bottom panel*). Next, quantitative PCR was used to measure LCAD mRNA in Cases 1–3 using the antigen-positive Case 2 as the reference for normalization. Compared with Case 2, Case 1 had ~40% less LCAD mRNA, whereas Case 3 was similar to Case 2. Genomic DNA was isolated from remaining lung tissue and used for sequencing the 11 LCAD exons and intron-exon boundaries. Cases 1 and 3 were both homozygous for a polymorphism that changes lysine residue 333 to glutamine. Case 2 was heterozygous for this polymorphism. No other mutations were detected.

DISCUSSION

These studies are the first to link FAO disorders to pulmonary lipid metabolism and lung dysfunction. Using human lung tissue and human primary cells, we demonstrated that the orphan FAO enzyme LCAD is enriched in surfactant-producing ATII cells. Subsequent mouse studies confirmed a physiological role for LCAD and the FAO pathway in lung. Lung FAO was found to be robust with rates of palmitate and oleate oxidation that rival that of the liver. LCAD knock-out mice showed reduced pulmonary compliance due to a paucity of large aggregate surfactant. Furthermore, the surfactant that is present in LCAD mice has altered molecular composition and a reduced ability to lower surface tension, and demonstrates greater compressibility.

In humans, surfactant deficiency manifests as respiratory distress syndrome (RDS), which is a major cause of mortality in children less than 1 year old (46). RDS is particularly common among premature infants because surfactant production by ATII cells occurs primarily in the final weeks of gestation. When surfactant deficiency occurs in term infants, the cause is often genetic. To date, LCAD has not been associated with RDS. However, RDS has been noted in several children deficient in mitochondrial trifunctional protein, the enzyme that functions just downstream of LCAD in the FAO pathway (47, 48). In one study of mitochondrial trifunctional protein patients, pneumonia and respiratory failure contributed to the deaths of six out of 13 patients followed (49). This link between mitochondrial trifunctional protein and respiratory failure suggests an important role for FAO in the lung. In this study, we evaluated post-mortem lung tissue from a small cohort of infants who suffered sudden unexplained deaths. Two of these cases had no detectable LCAD antigen. Sequencing revealed them both to be homozygous for a common single nucleotide polymorphism (rs2286963) resulting in an amino acid substitution (K333Q). In the dbSNP database (www.ncbi.nlm.nih.gov), 30.5% of 1270 individuals genotyped were heterozygous for K333Q, and 5.2% were homozygous. The probability of selecting two tissue samples at random that are homozygous for this polymorphism is ~1/400. Although no functional studies have been done for the K333Q variant, recent studies have linked it to increases in blood levels of C9-carnitine (50, 51). C9-carnitine is likely to be 2,6-dimethylheptanoyl-carnitine, a branched-chain acylcarnitine that would be predicted to accumulate in LCAD deficiency (5, 52). Future studies will determine the impact of the K333Q polymorphism on enzyme activity and stability, as well as establish the frequency of the polymorphism among cases of RDS and unexplained sudden infant deaths. We postulate that homozygosity for K333Q may increase the risk for infant mortality from pulmonary infections or other forms of alveolar stress.

Environmental or dietary factors may also suppress the FAO pathway in lung. For instance, conditions that deplete carnitine can severely limit FAO, which is carnitine-dependent. Lung cannot synthesize carnitine and must therefore transport it via

the transporter protein OCTN2 that is expressed in the alveolar epithelium (53). Besides carnitine, OCTN2 transports many cationic drugs, including ipratropium, which is an inhaled therapeutic for COPD and asthma (54). Competitive inhibition of OCTN2 by drugs can result in secondary carnitine deficiency (54). OCTN2 has been shown to be competitively inhibited to various degrees by dozens of drugs, including anti-cancer agents, β-lactam antibiotics, statins, β-blockers, antidepressants, and antihistamines, among others (55–58). The effects of these drugs on carnitine transport and FAO in the lung epithelium *in vivo* have not been established and require further investigation, especially in light of recent studies demonstrating carnitine deficiency in both children and adults with pulmonary disease (59–62).

The dominant phospholipid species in surfactant is dipalmitoyl-PC, which contains two 16-carbon saturated acyl chains (63). We have shown that disruption of LCAD in mice leads to changes in PC and PG composition as observed by mass spectrometry (Table 1), and these changes are associated with changes in surfactant behavior in the constrained drop surfactometer. To our knowledge, this is the first analysis of the phospholipid molecular species in the $LCAD^{-/-}$ mouse model. Previous studies have measured free fatty acids in the liver and serum acylcarnitines and noted an accumulation of 14-carbon lipids, particularly free C14:1 fatty acids and C14:1-carnitine (64). In contrast, the changes in surfactant composition reported here involve an increase in C18 to C22 chain lengths with varying degrees of unsaturation, and C14:1 was not detected in either PC or PG. Clearly, if C14:1 accumulates in lung of $LCAD^{-/-}$ mice, it is not incorporated into surfactant. Further work will be necessary to determine whether accumulating C14:1 may be elongated and further desaturated to produce the C18:1, C18:2, and C20:4 acyl chains observed in $LCAD^{-/-}$ surfactant or whether LCAD and the mitochondrial FAO pathway are important for chain-shortening C18–C22 fatty acids down to C16 acyl chains for incorporation into surfactant. Interestingly, mice deficient in the elongation of long-chain fatty acid family member 6 (Elovl6), an enzyme that elongates unsaturated fatty acids, are prone to lung fibrosis (65) suggesting that the proper mixture of phospholipid species is essential for pulmonary health.

Although the qualitative changes seen in $LCAD^{-/-}$ surfactant during dynamic cycling are most likely linked to the changes in phospholipid acyl chain composition, a clear mechanism is lacking for the quantitative change in surfactant phospholipids. The depletion in large aggregate surfactant phospholipids is probably the primary factor behind the reduced pulmonary compliance observed in $LCAD^{-/-}$ animals. This depletion is likely due to decreased surfactant synthesis or increased recycling/degradation. Our lung explant studies showed normal rates of choline incorporation into total lipid, but we did not investigate trafficking of lamellar bodies and extracellular release of surfactant material. With regard to degradation, we found no observable increase in PLA_2, which actively degrades phospholipids and is known to be increased in lavage fluid of children with RDS (66). Albumin, however, was consistently increased in $LCAD^{-/-}$ lavage fluid, and albumin has been shown to inactivate surfactant and to possess a phospholipase-like activity (67, 68). Loss of FAO as an energy source in ATI and ATII cells may compromise the integrity of the alveolar epithelium, leading to increased albumin and other proteins in the epithelial lining fluid, which may then inactivate or disrupt pulmonary surfactant. Further studies are underway to investigate these aspects of surfactant metabolism in $LCAD^{-/-}$ mice and to evaluate LCAD as a candidate gene for pulmonary disease in humans.

REFERENCES

1. Bartlett, K., and Eaton, S. (2004) Mitochondrial β-oxidation. *Eur. J. Biochem.* **271,** 462–469
2. Houten, S. M., and Wanders, R. J. (2010) A general introduction to the biochemistry of mitochondrial fatty acid β-oxidation. *J. Inherit. Metab. Dis.* **33,** 469–477
3. Wanders, R. J., Ruiter, J. P., IJLst, L., Waterham, H. R., and Houten, S. M. (2010) The enzymology of mitochondrial fatty acid β-oxidation and its application to follow-up analysis of positive neonatal screening results. *J. Inherit. Metab. Dis.* **33,** 479–494
4. He, M., Rutledge, S. L., Kelly, D. R., Palmer, C. A., Murdoch, G., Majumder, N., Nicholls, R. D., Pei, Z., Watkins, P. A., and Vockley, J. (2007) A new genetic disorder in mitochondrial fatty acid β-oxidation: ACAD9 deficiency. *Am. J. Hum. Genet.* **81,** 87–103
5. Wanders, R. J., Denis, S., Ruiter, J. P., IJlst, L., and Dacremont, G. (1998) 2,6-Dimethylheptanoyl-CoA is a specific substrate for long-chain acyl-CoA dehydrogenase (LCAD): Evidence for a major role of LCAD in branched-chain fatty acid oxidation. *Biochim. Biophys. Acta* **1393,** 35–40
6. Moczulski, D., Majak, I., and Mamczur, D. (2009) An overview of β-oxidation disorders. *Postepy Hig. Med. Dosw.* **63,** 266–277
7. Spiekerkoetter, U., Lindner, M., Santer, R., Grotzke, M., Baumgartner, M. R., Boehles, H., Das, A., Haase, C., Hennermann, J. B., Karall, D., de Klerk, H., Knerr, I., Koch, H. G., Plecko, B., Röschinger, W., Schwab, K. O., Scheible, D., Wijburg, F. A., Zschocke, J., Mayatepek, E., and Wendel, U. (2009) Management and outcome in 75 individuals with long-chain fatty acid oxidation defects: Results from a workshop. *J. Inherit. Metab. Dis.* **32,** 488–497
8. Nouws, J., Nijtmans, L., Houten, S. M., van den Brand, M., Huynen, M., Venselaar, H., Hoefs, S., Gloerich, J., Kronick, J., Hutchin, T., Willems, P., Rodenburg, R., Wanders, R., van den Heuvel, L., Smeitink, J., and Vogel, R. O. (2010) Acyl-CoA dehydrogenase 9 is required for the biogenesis of oxidative phosphorylation complex I. *Cell Metab.* **12,** 283–294
9. Haack, T. B., Danhauser, K., Haberberger, B., Hoser, J., Strecker, V., Boehm, D., Uziel, G., Lamantea, E., Invernizzi, F., Poulton, J., Rolinski, B., Iuso, A., Biskup, S., Schmidt, T., Mewes, H. W., Wittig, I., Meitinger, T., Zeviani, M., Prokisch, H. (2010) Exome sequencing identifies ACAD9 mutations as a cause of complex I deficiency. *Nat. Genet.* **42,** 1131–1134
10. Maher, A. C., Mohsen, A. W., Vockley, J., and Tarnopolsky, M. A. (2010) Low expression of long-chain acyl-CoA dehydrogenase in human skeletal muscle. *Mol. Genet. Metab.* **100,** 163–167
11. Chegary, M., Brinke Ht, Ruiter, J. P., Wijburg, F. A., Stoll, M. S., Minkler, P. E., van Weeghel, M., Schulz, H., Hoppel, C. L., Wanders, R. J., and Houten, S. M. (2009) Mitochondrial long chain fatty acid β-oxidation in man and mouse. *Biochim. Biophys. Acta* **1791,** 806–815
12. Wang, J., Nikrad, M. P., Phang, T., Gao, B., Alford, T., Ito, Y., Edeen, K., Travanty, E. A., Kosmider, B., Hartshorn, K., and Mason, R. J. (2011) Innate immune response to influenza A virus in differentiated human alveolar type II cells. *Am. J. Respir. Cell Mol. Biol.* **45,** 582–591
13. Hou, J., Aerts, J., den Hamer, B., van Ijcken, W., den Bakker, M., Riegman, P., van der Leest, C., van der Spek, P., Foekens, J. A., Hoogsteden, H. C., Grosveld, F., and Philipsen, S. (2010) Gene expression-based classification of non-small cell lung carcinomas and survival prediction. *PLoS One* **5,** e10312
14. Kosmider, B., Messier, E. M., Janssen, W. J., Nahreini, P., Wang, J., Hartshorn, K. L., and Mason, R. J. (2012) Nrf2 protects human alveolar epithelial cells against injury induced by influenza A virus. *Respir. Res.* **13,** 43
15. Kosmider, B., Messier, E. M., Chu, H. W., and Mason, R. J. (2011) Human

alveolar epithelial cell injury induced by cigarette smoke. *PLoS One* **6,** e26059
16. Wang, J., Edeen, K., Manzer, R., Chang, Y., Wang, S., Chen, X., Funk, C. J., Cosgrove, G. P., Fang, X., and Mason, R. J. (2007) Differentiated human alveolar epithelial cells and reversibility of their phenotype *in vitro*. *Am. J. Respir. Cell Mol. Biol.* **36,** 661–668
17. Zhou, J., You, Y., Ryan, A. J., and Mallampalli, R. K. (2004) Upregulation of surfactant synthesis triggers ABCA1-mediated basolateral phospholipid efflux. *J. Lipid Res.* **45,** 1758–1767
18. Mendez-Figueroa, H., Chien, E. K., Ji, H., Nesbitt, N. L., Bharathi, S. S., and Goetzman, E. (2013) Effects of labor on placental fatty acid β oxidation. *J. Matern. Fetal Neonatal. Med.* **26,** 150–154
19. Goetzman, E. S. (2009) The regulation of acyl-CoA dehydrogenases in adipose tissue by rosiglitazone. *Obesity* **17,** 196–198
20. DeBuysere, M. S., and Olson, M. S. (1983) The analysis of acyl-coenzyme A derivatives by reverse-phase high-performance liquid chromatography. *Anal. Biochem.* **133,** 373–379
21. Bligh, E. G., and Dyer, W. J. (1959) A rapid method of total lipid extraction and purification. *Can. J. Biochem. Physiol.* **37,** 911–917
22. Alcorn, J. F., Ckless, K., Brown, A. L., Guala, A. S., Kolls, J. K., Poynter, M. E., Irvin, C. G., van der Vliet, A., and Janssen-Heininger, Y. M. (2010) Strain-dependent activation of NF-κB in the airway epithelium and its role in allergic airway inflammation. *Am. J. Physiol. Lung Cell Mol. Physiol.* **298,** L57–L66
23. Bates, J. H., and Irvin, C. G. (2003) Measuring lung function in mice: the phenotyping uncertainty principle. *J. Appl. Physiol.* **94,** 1297–1306
24. Bartlett, G. R. (1959) Phosphorus assay in column chromatography. *J. Biol. Chem.* **234,** 466–468
25. Mallampalli, R. K., Ryan, A. J., Salome, R. G., and Jackowski, S. (2000) Tumor necrosis factor-α inhibits expression of CTP:phosphocholine cytidylyltransferase. *J. Biol. Chem.* **275,** 9699–9708
26. Zuo, Y. Y., Acosta, E., Policova, Z., Cox, P. N., Hair, M. L., and Neumann, A. W. (2006) Effect of humidity on the stability of lung surfactant films adsorbed at air-water interfaces. *Biochim. Biophys. Acta* **1758,** 1609–1620
27. Zuo, Y. Y., Alolabi, H., Shafiei, A., Kang, N., Policova, Z., Cox, P. N., Acosta, E., Hair, M. L., and Neumann, A. W. (2006) Chitosan enhances the *in vitro* surface activity of dilute lung surfactant preparations and resists albumin-induced inactivation. *Pediatr. Res.* **60,** 125–130
28. Yu, L. M., Lu, J. J., Chan, Y. W., Ng, A., Zhang, L., Hoorfar, M., Policova, Z., Grundke, K., and Neumann, A. W. (2004) Constrained sessile drop as a new configuration to measure low surface tension in lung surfactant systems. *J. Appl. Physiol.* **97,** 704–715
29. Schürch, S., Bachofen, H., Goerke, J., and Possmayer, F. (1989) A captive bubble method reproduces the *in situ* behavior of lung surfactant monolayers. *J. Appl. Physiol.* **67,** 2389–2396
30. Schürch, S., Bachofen, H., Goerke, J., and Green, F. (1992) Surface properties of rat pulmonary surfactant studied with the captive bubble method: adsorption, hysteresis, stability. *Biochim. Biophys. Acta* **1103,** 127–136
31. Zuo, Y. Y., Ding, M., Li, D., and Neumann, A. W. (2004) Further development of axisymmetric drop shape analysis–Captive bubble for pulmonary surfactant related studies. *Biochim. Biophys. Acta* **1675,** 12–20
32. Folch, J., Lees, M., and Sloane Stanley, G. H. (1957) A simple method for the isolation and purification of total lipids from animal tissues. *J. Biol. Chem.* **226,** 497–509
33. Tyurina, Y. Y., Kisin, E. R., Murray, A., Tyurin, V. A., Kapralova, V. I., Sparvero, L. J., Amoscato, A. A., Samhan-Arias, A. K., Swedin, L., Lahesmaa, R., Fadeel, B., Shvedova, A. A., and Kagan, V. E. (2011) Global phospholipidomics analysis reveals selective pulmonary peroxidation profiles upon inhalation of single-walled carbon nanotubes. *ACS Nano* **5,** 7342–7353
34. Böttcher, C. J. F., Van gent, C. M. and Pries, C. (1961) A rapid and sensitive sub-micro phosphorus determination. *Anal. Chim. Acta* **24,** 203
35. Juaneda, P., and Rocquelin, G. (1985) Rapid and convenient separation of phospholipids and nonphosphorus lipids from rat heart using silica cartridges. *Lipids* **20,** 40–41
36. Schulz, H. (1994) Regulation of fatty acid oxidation in heart. *J. Nutr.* **124,** 165–171
37. Wanders, R. J., Ferdinandusse, S., Brites, P., and Kemp, S. (2010) Peroxisomes, lipid metabolism and lipotoxicity. *Biochim. Biophys. Acta* **1801,** 272–280
38. Parker, J. C., and Townsley, M. I. (2004) Evaluation of lung injury in rats and mice. *Am. J. Physiol. Lung Cell Mol. Physiol.* **286,** L231–L246
39. Kim, K. J., and Malik, A. B. (2003) Protein transport across the lung epithelial barrier. *Am. J. Physiol. Lung Cell Mol. Physiol.* **284,** L247–L259
40. Ikegami, M., Korfhagen, T. R., Whitsett, J. A., Bruno, M. D., Wert, S. E., Wada, K., and Jobe, A. H. (1998) Characteristics of surfactant from SP-A-deficient mice. *Am. J. Physiol.* **275,** L247–L254
41. Saad, S. M., Policova, Z., Acosta, E. J., and Neumann, A. W. (2012) Effect of surfactant concentration, compression ratio and compression rate on the surface activity and dynamic properties of a lung surfactant. *Biochim. Biophys. Acta* **1818,** 103–116
42. Chintagari, N. R., Mishra, A., Su, L., Wang, Y., Ayalew, S., Hartson, S. D., and Liu, L. (2010) Vacuolar ATPase regulates surfactant secretion in rat alveolar type II cells by modulating lamellar body calcium. *PLoS One* **5,** e9228
43. De Luca, D., Capoluongo, E., and Rigo, V. (2011) Secretory phospholipase A2 pathway in various types of lung injury in neonates and infants: A multicentre translational study. *BMC Pediatr.* **11,** 101
44. Niewoehner, D. E., Rice, K., Duane, P., Sinha, A. A., Gebhard, R., and Wangensteen, D. (1989) Induction of alveolar epithelial injury by phospholipase A2. *J. Appl. Physiol.* **66,** 261–267
45. Boles, R. G., Buck, E. A., Blitzer, M. G., Platt, M. S., Cowan, T. M., Martin, S. K., Yoon, H., Madsen, J. A., Reyes-Mugica, M., and Rinaldo, P. (1998) Retrospective biochemical screening of fatty acid oxidation disorders in postmortem livers of 418 cases of sudden death in the first year of life. *J. Pediatr.* **132,** 924–933
46. Blank, R., and Napolitano, L. M. (2011) Epidemiology of ARDS and ALI. *Crit. Care Clin.* **27,** 439–458
47. Lundy, C. T., Shield, J. P., Kvittingen, E. A., Vinorum, O. J., Trimble, E. R., and Morris, A. A. (2003) Acute respiratory distress syndrome in long-chain 3-hydroxyacyl-CoA dehydrogenase and mitochondrial trifunctional protein deficiencies. *J. Inherit. Metab. Dis.* **26,** 537–541
48. Das, A. M., Illsinger, S., Lücke, T., Hartmann, H., Ruiter, J. P., Steuerwald, U., Waterham, H. R., Duran, M., and Wanders, R. J. (2006) Isolated mitochondrial long-chain ketoacyl-CoA thiolase deficiency resulting from mutations in the HADHB gene. *Clin. Chem.* **52,** 530–534
49. Tyni, T., Palotie, A., Viinikka, L., Valanne, L., Salo, M. K., von Döbeln, U., Jackson, S., Wanders, R., Venizelos, N., and Pihko, H. (1997) Long-chain 3-hydroxyacyl-coenzyme A dehydrogenase deficiency with the G1528C mutation: Clinical presentation of thirteen patients. *J. Pediatr.* **130,** 67–76
50. Hong, M. G., Karlsson, R., Magnusson, P. K., Lewis, M. R., Isaacs, W., Zheng, L. S., Xu, J., Grönberg, H., Ingelsson, E., Pawitan, Y., Broeckling, C., Prenni, J. E., Wiklund, F., and Prince, J. A. (2013) A genome-wide assessment of variability in human serum metabolism. *Hum. Mutat.* **34,** 515–524
51. Illig, T., Gieger, C., Zhai, G., Römisch-Margl, W., Wang-Sattler, R., Prehn, C., Altmaier, E., Kastenmüller, G., Kato, B. S., Mewes, H. W., Meitinger, T., de Angelis, M. H., Kronenberg, F., Soranzo, N., Wichmann, H. E., Spector, T. D., Adamski, J., and Suhre, K. (2010) A genome-wide perspective of genetic variation in human metabolism. *Nat. Genet.* **42,** 137–141
52. Verhoeven, N. M., Roe, D. S., Kok, R. M., Wanders, R. J., Jakobs, C., and Roe, C. R. (1998) Phytanic acid and pristanic acid are oxidized by sequential peroxisomal and mitochondrial reactions in cultured fibroblasts. *J. Lipid Res.* **39,** 66–74
53. Horvath, G., Schmid, N., Fragoso, M. A., Schmid, A., Conner, G. E., Salathe, M., and Wanner, A. (2007) Epithelial organic cation transporters ensure pH-dependent drug absorption in the airway. *Am. J. Respir. Cell Mol. Biol.* **36,** 53–60
54. Tamai, I. (2013) Pharmacological and pathophysiological roles of carnitine/organic cation transporters (OCTNs: SLC22A4, SLC22A5, and Slc22a21). *Biopharm. Drug Dispos.* **34,** 29–44
55. Hu, C., Lancaster, C. S., Zuo, Z., Hu, S., Chen, Z., Rubnitz, J. E., Baker, S. D., and Sparreboom, A. (2012) Inhibition of OCTN2-mediated transport of carnitine by etoposide. *Mol. Cancer Ther.* **11,** 921–929
56. Zheng, X., Diao, L., Ekins, S., and Polli, J. E. (2010) Why we should be vigilant: Drug cytotoxicity observed with *in vitro* transporter inhibition

studies. *Biochem. Pharmacol.* **80,** 1087–1092
57. Diao, L., Ekins, S., and Polli, J. E. (2009) Novel inhibitors of human organic cation/carnitine transporter (hOCTN2) via computational modeling and *in vitro* testing. *Pharm. Res.* **26,** 1890–1900
58. Ganapathy, M. E., Huang, W., Rajan, D. P., Carter, A. L., Sugawara, M., Iseki, K., Leibach, F. H., and Ganapathy, V. (2000) β-Lactam antibiotics as substrates for OCTN2, an organic cation/carnitine transporter. *J. Biol. Chem.* **275,** 1699–1707
59. Asilsoy, S., Bekem, O., Karaman, O., Uzuner, N., and Kavukçu, S. (2009) Serum total and free carnitine levels in children with asthma. *World J. Pediatr.* **5,** 60–62
60. Borghi-Silva, A., Baldissera, V., Sampaio, L. M., Pires-DiLorenzo, V. A., Jamami, M., Demonte, A., Marchini, J. S., and Costa, D. (2006) L-Carnitine as an ergogenic aid for patients with chronic obstructive pulmonary disease submitted to whole-body and respiratory muscle training programs. *Braz. J. Med. Biol. Res.* **39,** 465–474
61. Korkmaz, A., Tekinalp, G., Coskun, T., Yigit, S., and Yurdakok, M. (2005) Plasma carnitine levels in preterm infants with respiratory distress syndrome. *Pediatr. Int.* **47,** 49–52
62. Törel Ergür, A., Tanzer, F., and Cetinkaya, O. (1997) Serum free carnitine levels in children with recurrent pulmonary infections. *Acta Paediatr. Jpn.* **39,** 406–408
63. Perez-Gil, J., and Weaver, T. E. (2010) Pulmonary surfactant pathophysiology: Current models and open questions. *Physiology* **25,** 132–141
64. Cox, K. B., Hamm, D. A., Millington, D. S., Matern, D., Vockley, J., Rinaldo, P., Pinkert, C. A., Rhead, W. J., Lindsey, J. R., and Wood, P. A. (2001) Gestational, pathologic and biochemical differences between very long-chain acyl-CoA dehydrogenase deficiency and long-chain acyl-CoA dehydrogenase deficiency in the mouse. *Hum. Mol. Genet.* **10,** 2069–2077
65. Sunaga, H., Matsui, H., Ueno, M., Maeno, T., Iso, T., Syamsunarno, M. R., Anjo, S., Matsuzaka, T., Shimano, H., Yokoyama, T., and Kurabayashi, M. (2013) Deranged fatty acid composition causes pulmonary fibrosis in Elovl6-deficient mice. *Nat. Commun.* **4,** 2563
66. Kitsiouli, E., Nakos, G., and Lekka, M. E. (2009) Phospholipase A2 subclasses in acute respiratory distress syndrome. *Biochim. Biophys. Acta* **1792,** 941–953
67. Damas, J. E., and Cake, M. H. (2011) An albumin-associated PLA2-like activity inactivates surfactant phosphatidylcholine secreted from fetal type II pneumocytes. *Am. J. Physiol. Lung Cell Mol. Physiol.* **301,** L966–L974
68. Zuo, Y. Y., Tadayyon, S. M., Keating, E., Zhao, L., Veldhuizen, R. A., Petersen, N. O., Amrein, M. W., and Possmayer, F. (2008) Atomic force microscopy studies of functional and dysfunctional pulmonary surfactant films, II: Albumin-inhibited pulmonary surfactant films and the effect of SP-A. *Biophys. J.* **95,** 2779–2791
69. Bharathi, S. S., Zhang, Y., Mohsen, A. W., Uppala, R., Balasubramani, M., Schreiber, E., Uechi, G., Beck, M. E., Rardin, M. J., Vockley, J., Verdin, E., Gibson, B. W., Hirschey, M. D., and Goetzman, E. S. (2013) Sirtuin 3 (SIRT3) protein regulates long-chain acyl-CoA dehydrogenase by deacetylating conserved lysines near the active site. *J. Biol. Chem.* **288,** 33837–33847